Electronic states of dibenzo-p-dioxin

A synchrotron radiation linear dichroism Investigation.

Nguyen, Duy Duc; Jones, Nykola C.; Hoffmann, Søren V.; Spanget-Larsen, Jens

Published in:
Chemical Physics

DOI:
10.1016/j.chemphys.2018.12.003

Publication date:
2019

Document Version
Peer reviewed version

Citation for published version (APA):
Nguyen, D. D., Jones, N. C., Hoffmann, S. V., & Spanget-Larsen, J. (2019). Electronic states of dibenzo-*p*-dioxin: A synchrotron radiation linear dichroism Investigation. *Chemical Physics*, *519*, 64-68. https://doi.org/10.1016/j.chemphys.2018.12.003

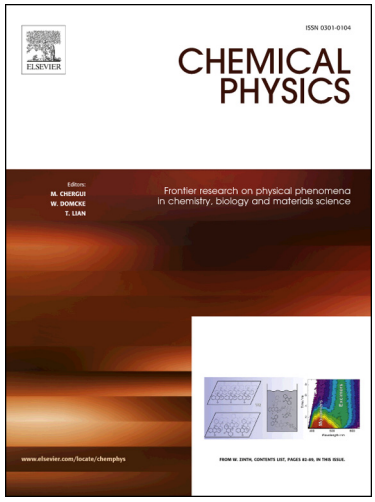

Electronic states of dibenzo-*p* –dioxin. A synchrotron radiation linear dichroism Investigation

Duy Duc Nguyen, Nykola C. Jones, Søren V. Hoffmann, Jens Spanget–Larsen

PII: S0301-0104(18)31235-7
DOI: https://doi.org/10.1016/j.chemphys.2018.12.003
Reference: CHEMPH 10256

To appear in: *Chemical Physics*

Received Date: 7 November 2018
Revised Date: 7 December 2018
Accepted Date: 7 December 2018

Please cite this article as: D.D. Nguyen, N.C. Jones, S.V. Hoffmann, J. Spanget–Larsen, Electronic states of dibenzo-*p* –dioxin. A synchrotron radiation linear dichroism Investigation, *Chemical Physics* (2018), doi: https://doi.org/10.1016/j.chemphys.2018.12.003

Electronic states of dibenzo-*p*-dioxin. A synchrotron radiation linear dichroism Investigation.

Duy Duc Nguyen[a,#], Nykola C. Jones[b], Søren V. Hoffmann[b], Jens Spanget-Larsen[a,*]

[a] *Department of Science and Environment, Roskilde University, Universitetsvej 1, DK-4000 Roskilde, Denmark.*

[b] *ISA, Department of Physics and Astronomy, Aarhus University, Ny Munkegade 120, Bldg. 1520, DK-8000 Aarhus C, Denmark*

Keywords

Dibenzo-*p*-dioxin
Linear dichroism (LD)
Polarization directions
Near and vacuum UV
Synchrotron radiation
Stretched polyethylene
Time-dependent density functional theory (TD-DFT)

[#] Present Address:
Duy Duc Nguyen, Intertek Vietnam Limited, 5th, 6th, 7th floor of Lobby D at S.O.H.O Biz Office Building, No. 38 Huynh Lan Khanh St., Ward 2, Tan Binh District, Ho Chi Minh City, Vietnam.

* Corresponding Author
E-mail address: Spanget@ruc.dk (J. Spanget-Larsen)

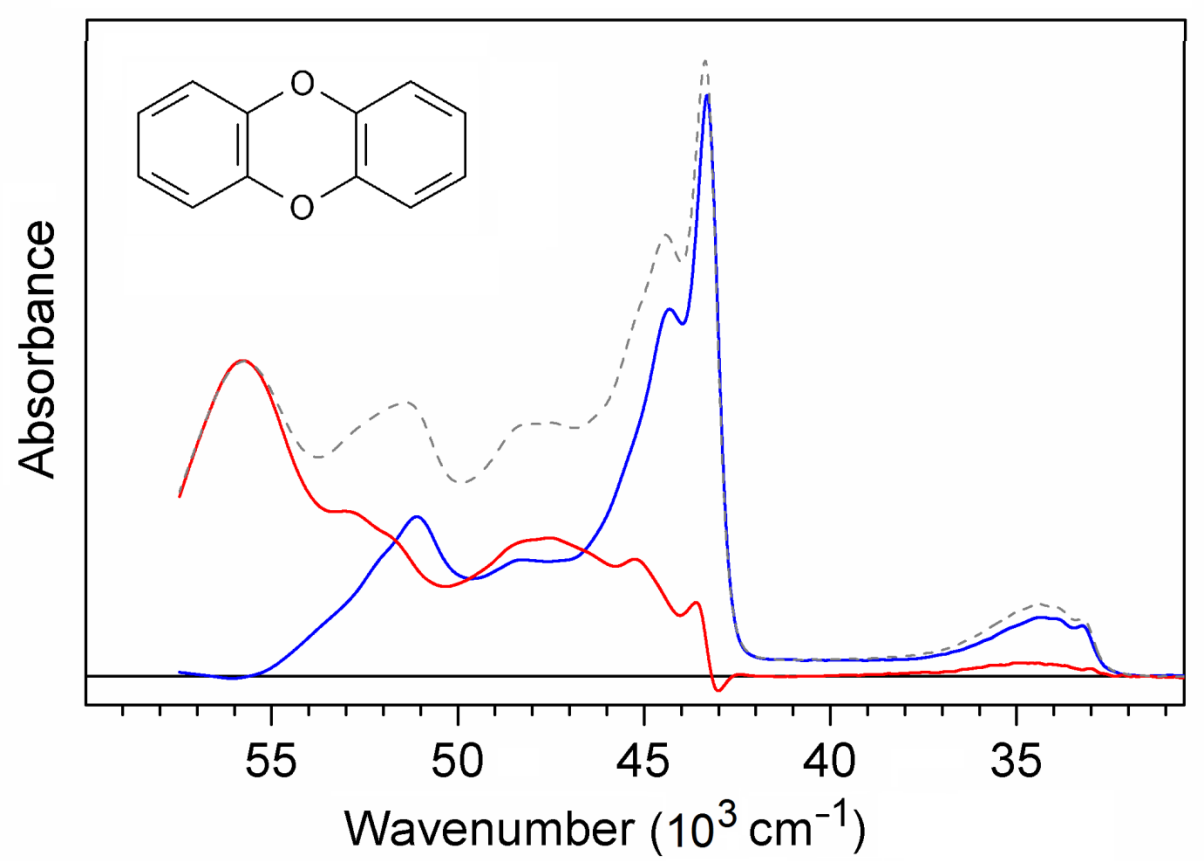

Graphical abstract

Highlights

- UV absorbance spectra of dibenzo-*p*-dioxin measured with synchrotron radiation
- Polarization spectroscopy in the near and vacuum UV spectral regions
- Linear dichroism enables experimental symmetry assignment of molecular states
- Revision of previous assignments of the excited singlet states of dibenzo-*p*-dioxin
- Electronic transitions predicted with time-dependent density functional theory

ABSTRACT. The UV absorbance bands of dibenzo-*p*-dioxin (dibenzo-1,4-dioxin, DD) are investigated by synchrotron radiation linear dichroism (SRLD) spectroscopy on molecular samples aligned in stretched polyethylene. The investigation covers the range 58000–30000 cm^{-1} (170–330 nm), thereby providing new information on the transitions of DD in the vacuum UV region. The observed polarization data enable experimental symmetry assignments of the observed transitions, leading to revision of previously published assignments by Ljubić and Sabljić (J. Phys. Chem. A 109 (2005) 8209-8217). In general, the experimental spectra are well predicted by the results of quantum chemical calculations using time-dependent density functional theory (TD–DFT). The observed absorbance in the region 58000–55000 cm^{-1} (170–180 nm) in the vacuum UV is almost entirely short-axis polarized, in pleasing agreement with the predicted spectrum.

1. Introduction

"Dioxins" is a class of chemicals that causes serious concern as persistent organic pollutants in the environment [1-8]. The most harmful dioxins are believed to be halogen derivatives of dibenzo-*p*-dioxin (DD, Chart 1) and these compounds have attracted particular attention. The molecular and electronic structure of DD and its derivatives have thus been studied by several authors [9-22].

The most advanced theoretical study of the electronic states of parent DD is probably the one published in 2005 by Ljubić and Sabljić [16]. They computed several valence excited states by using *ab initio* multi-configurational CASSCF/CASPT2 theory. The predicted transitions to excited singlet states were compared with the observed near-UV absorption spectrum of DD in an isopentane matrix at 77 K [10-12]. However, the comparison was not entirely satisfactory and the authors produced a "theoretically fitted" curve empirically adjusted to reproduce the appearance of the observed absorbance curve [16].

The aim of the present publication is to resolve some of the discrepancies by providing additional experimental evidence. In this work, we investigate the UV absorption spectrum of DD by synchrotron radiation linear dichroism (SRLD) spectroscopy on molecular samples partially aligned in stretched polyethylene (PE). Compared with traditional absorption spectroscopy, SRLD spectroscopy provides two significant advantages. In the first place, linear dichroism (LD) spectroscopy [23-26] on oriented molecular assemblies yields information on the polarization directions of the recorded absorption bands, thereby frequently providing an experimental symmetry assignment of the observed molecular states. Secondly, the use of synchrotron radiation [27,28] enables a substantial expansion of the investigated spectral range, compared with the use of a traditional light source [29-33]. In the present investigation, the measurement is thus extended into the vacuum UV, covering the region up to 58000 cm^{-1} (170 nm). This is an extension of the previously investigated spectral range [10-12] by about 10000 cm^{-1}. The observed absorption bands are discussed with

reference to theoretical transitions predicted with time dependent density functional theory (TD-DFT) calculations [34-36]. Additional information is provided as Supplementary data, referred to in the ensuing text as S1 and S2.

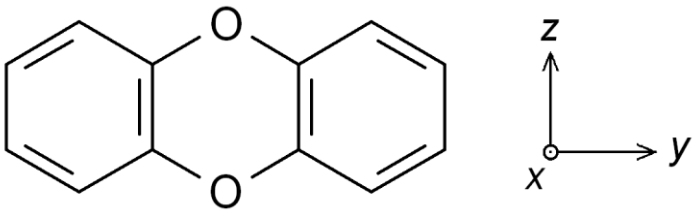

Scheme 1. Dibenzo-*p*-dioxin (DD) with definition of the molecular coordinate system.

2. Experimental

2.1 Sample Preparation

A sample of dibenzo-*p*-dioxin (DD) was purchased from TCI Europe n.v. (purity >99%). Low-density polyethylene (PE) 100μm sheet material without any additives was obtained from Hinnum Plast A/S. A 2.5×6 cm PE piece cut from the sheet was washed with chloroform (Merck Uvasol) at 50 °C for one day to extract possible impurities. DD was then introduced into the dried PE sample from a saturated solution of the substance in chloroform. Subsequently, the chloroform was allowed to evaporate from the doped sample and crystalline deposits on the surface were removed with ethanol (Merck Uvasol). The sample was finally uniaxially stretched by approximately 500%. A reference sample without solute was produced in the same manner. Further details on stretched polyethylene samples can be found in the literature [23,24].

2.2 Linear Dichroism (LD) Spectroscopy

SRLD spectra were measured at room temperature as previously described [29-33] on the CD1 beamline [27,28] at the storage ring ASTRID at the Centre for Storage Ring Facilities (ISA). Two absorbance curves were recorded with the electric vector of the sample beam parallel (U) and perpendicular (V) to the stretching direction of the PE polymer. The

observed baseline-corrected LD absorbance curves $E_U(\tilde{\nu})$ and $E_V(\tilde{\nu})$ are shown in Fig. 1 (top).

3. Calculations

Quantum chemical calculations were performed by using the GAUSSIAN16 software package [37]. The ground state equilibrium geometry of DD was computed by using B3LYP [38-40] DFT and the cc-pVTZ basis set by Dunning and co-workers [41,42]. The molecule is predicted to have D_{2h} symmetrical nuclear configuration, in consistency with the results of previous investigations [13-18]. The computed nuclear coordinates are provided as Supplementary data S1. Vertical electronic transitions from the ground state to excited singlet states were computed with the TD-DFT [34-36] procedure by using the long range-corrected functional CAM-B3LYP [43] and the basis set aug-cc-pVTZ [41,42]. A constant term was subtracted from the computed wavenumbers in order to facilitate comparison of observed and predicted trends [44]; an empirical correction of 4000 cm^{-1} was found to be adequate for transitions predicted with TD–CAM-B3LYP [32,33]. The main calculated transitions are listed in Table 1, a full listing is provided as Supplementary data S2. Gaussian convolutions of the predicted transitions were computed by representing the contribution due to the *i*'th transition by the following expression [45]:

$$\varepsilon_i(\tilde{\nu}) = \frac{2.175 \cdot 10^8}{w} \cdot f_i \cdot \exp\left[-2.772\left(\frac{\tilde{\nu}-\tilde{\nu}_i}{w}\right)^2\right] \qquad (1)$$

where $\varepsilon_i(\tilde{\nu})$ = molar absorption coefficient (L mol^{-1} cm^{-1}) as a function of wavenumber (cm^{-1}), $\tilde{\nu}_i$ = predicted vertical wavenumber, f_i = predicted oscillator strength, and w = full width at half height, taken as 3000 cm^{-1}. The resulting convoluted curves corresponding to transitions to states of B_{1u}, B_{2u}, and B_{3u} symmetry in the D_{2h} point group are shown in Fig. 2 (bottom).

4. Results and Discussion

4.1 Linear Dichroism: Orientation Factors and Partial Absorbance Curves

The observed SRLD absorption curves $E_U(\tilde{\nu})$ and $E_V(\tilde{\nu})$ for DD partially aligned in stretched PE are shown in Fig. 1 (top). Relative to traditional spectroscopy on isotropic samples, the additional information that can be extracted from the LD curves is represented by the orientation factors K_i for the moments of the observed transitions i [23-26]:

$$K_i = \langle \cos^2(\vec{M}_i, U) \rangle \qquad (2)$$

Here $(\vec{M}_i, U)$ is the angle of the transition moment vector $\vec{M}_i$ of transition i with the stretching direction U of the polymer. The pointed brackets indicate an average over all solute molecules in the light path. The orientation factors K_i may be determined by the graphical TEM (Trial and Error Method) stepwise reduction procedure [23,24] which involves construction of linear combinations of $E_U(\tilde{\nu})$ and $E_V(\tilde{\nu})$. Here we consider the reduced absorbance curves $r_K(\tilde{\nu})$ [46]:

$$r_K(\tilde{\nu}) = (1 - K)E_U(\tilde{\nu}) - 2KE_V(\tilde{\nu}) \qquad (3)$$

A family of curves $r_K(\tilde{\nu})$ for DD is shown in Fig. 1. A spectral feature due to transition i vanishes from the linear combination $r_K(\tilde{\nu})$ for $K = K_i$ and the K_i value may thus be determined by visual inspection. In the present case of molecular D_{2h} symmetry, allowed transitions must be polarized along the three symmetry axes x, y, and z, corresponding to excited states of B_{3u}, B_{2u}, and B_{1u} symmetry, respectively. Within experimental error, we thus expect to observe only three different K_i values equal to K_x, K_y, and K_z, and the three characteristic values should add up to unity [23-26]. In the previously published FTIR-LD investigation of DD partially aligned in stretched PE the following orientation factors were determined: (K_x, K_y, K_z) = (0.130 ± 0.005, 0.60 ± 0.01, 0.26 ± 0.01) [18]. From the curves in Fig. 1 we obtain K = 0.60 for the peaks at 34000 and 43000 cm^{-1} and a value close to 0.25 can be estimated for the band peaking at 55900 cm^{-1}. These K values must evidently be assigned to K_y and K_z, indicating absorption due to transitions polarized along the in-plane

long and short molecular axes *y* and *z*. We shall assume that absorbance polarized along the out-of-plane *x* axis is negligible in the observed spectral range; this assumption is confirmed by the calculated transitions, see Table 1, Fig. 2 (bottom), and S2. It is then possible to construct the partial absorbance curves $A_y(\tilde{\nu})$ and $A_z(\tilde{\nu})$ corresponding to *y*- and *z*-polarized intensity, respectively [46]:

$$A_y(\tilde{\nu}) = \left(K_y - K_z\right)^{-1} \cdot r_{K_z}(\tilde{\nu}) \qquad (4)$$
$$A_z(\tilde{\nu}) = (K_z - K_y)^{-1} \cdot r_{K_y}(\tilde{\nu})$$

The curves $A_y(\tilde{\nu})$ and $A_z(\tilde{\nu})$ produced with (K_y, K_z) = (0.60, 0.25) are shown in Fig. 2 (top). Four long-axis (*y*) polarized features *A*, *B*, *D*, and *E* and three short-axis (*z*) polarized features *C*, *F*, and *G* are indicated. The observed wavenumbers, relative absorbances, and polarization directions are listed in Table 1.

4.2 Electronic transitions

The observed partial absorbance spectra are compared with the predicted transitions in Table 1 and in Fig. 2. The spectrum starts with a medium intense band *A* with a maximum at 34200 cm^{-1} and a feature close to 33200 cm^{-1} which may correspond to the onset of the band. Band *A* is predominantly long-axis (*y*) polarized, overlapping weaker, short-axis polarized absorbance. We assign the long-axis polarized intensity to the 1 $^1B_{2u}$ π–π∗ state predicted at 34400 cm^{-1} with oscillator strength *f* = 0.11 (Table 1). The short-axis polarized intensity may be due to the optically forbidden π–π∗ states 1 $^1B_{3g}$ and 2 ^1A_g predicted at 32200 and 33000 cm^{-1}, possibly obtaining intensity by distortions of the molecular geometry and by vibronic coupling with the 1 $^1B_{2u}$ state.

This assignment is at variance with the one suggested by Ljubić and Sabljić [16]. In the cryogenic matrix spectrum considered by these authors, two features of band *A* are observed near 33300 cm^{-1} (300 nm) and 35100 cm^{-1} (286 nm). They assigned the first feature to the 1 $^1B_{2u}$ state, but they assumed that the major part of the intensity of band *A* was due to the 2 ^1A_g state, responsible for the observed maximum of the band. The authors suggested that the 2 ^1A_g

state gained optical intensity because of distortion of the molecular geometry of DD in the condensed phase to a "butterfly" conformation with C_{2v} symmetry [16]. However, transition to the $2\ ^1A_1$ state in the distorted conformation would be "out-of-plane" polarized, in disagreement with the observed long-axis polarized intensity. Ljubić and Sabljić [16] found a large inconsistency between the observed intensity of band *A* and the oscillator strength predicted with CASSCF/CASPT2 for the $2\ ^1A_1$ state in a mildly folded conformation. They characterized this inconsistency as a "large discrepancy", suspecting that another mechanism might be responsible for the intensity gain. The present reassignment of band *A* resolves the discrepancy.

The strong band *B* has a sharp peak at 43300 cm^{-1} and a component at 44200 cm^{-1} (Fig. 2). The band is *y*-polarized band and is easily assigned to the $2\ ^1B_{2u}$ $\pi-\pi*$ state computed at 43900 cm^{-1} with $f = 0.93$. Two well-resolved features of band *B* are also observed in the low-temperature matrix spectrum considered by Ljubić and Sabljić [16], near 43200 cm^{-1} (221 nm) and 46700 cm^{-1} (214 nm). These authors assigned the two features to two different electronic states, $2\ ^1B_{2u}$ and $2\ ^1B_{1u}$, respectively. But assignment of the second feature to $2\ ^1B_{1u}$ seems unlikely since the corresponding peak is *y*-polarized in the stretched PE spectrum. This feature is probably due to a vibronic component of band *B*, involving a totally symmetric vibrational mode. Inspection of Fig. 2 (top) shows that the peaks at 43300 and 44200 cm^{-1} in the partial absorbance curve $A_y(\tilde{\nu})$ are associated with S-shaped "wiggles" in the curve $A_z(\tilde{\nu})$. This phenomenon is frequently observed in reduction procedures with sharp peaks and can be explained by orientation-dependent inhomogeneous line-broadening (different solvent effects for differently oriented solute molecules) [23,24].

The high-energy region of the spectrum is very complex, with broad and overlapping long- and short-axis polarized band systems. Our assignment of observed features in this region to calculated electronic transitions is necessarily tentative.

Short-axis (*z*) polarized features *C*, *F*, and *G* are observed at 47600, 52900, and 55900 cm^{-1}. *C* and *F* can possibly be assigned to the π–π* states 2 $^1B_{1u}$ and 3 $^1B_{1u}$ predicted at 48100 and 51800 cm^{-1} (Table 1). Band *G* peaking at 55900 cm^{-1} in the vacuum UV may be due to overlapping contributions from the two states 5 $^1B_{1u}$ and 6 $^1B_{1u}$ computed at 55800 and 57600 cm^{-1}. This region of the observed spectrum is almost entirely *z*-polarized, in pleasing agreement with the predicted spectrum (Table 1, Fig. 2).

Long-axis (*y*) polarized bands *D* and *E* are observed with maxima at 48300 and 51000 cm^{-1}. The feature *E* at 51000 cm^{-1} can probably be assigned to contributions from the 3 $^1B_{2u}$ and 4 $^1B_{2u}$ states predicted at 51200 and 52100 cm^{-1}. The present theoretical results offer no obvious assignment of the absorption *D* with maximum at 48300 cm^{-1}. This absorption may be of vibronic origin, possibly involving the strong, long-axis polarized bands *B* and *E* with maxima at 43300 and 51000 cm^{-1}. On the other hand, the apparent failure to predict an electronic state corresponding to band *D* may also be due to shortcomings of the applied TD-DFT procedure, which may be less reliable in the high-energy region.

5. Conclusions

In this study, polarization data for DD is provided by SRLD polarization spectroscopy in the region 58000–30000 cm^{-1} (170–300 nm), leading to the observation of four long-axis and three short-axis polarized major features. The results demonstrate the usefulness of LD spectroscopy in the assignment of electronic transitions to molecular states. The observed polarization directions thus lead to experimental symmetry assignments of the observed transitions, thereby suggesting revision of previous assignments by Ljubić and Sabljić [16]. According to these authors, the bulk of the intensity of the first medium intense absorbance band *A*, with maximum observed at 34200 cm^{-1} (292 nm) in the present work, is due to the 2 ^1A_g state, presumably gaining optical intensity by distortion of the molecular geometry to a "butterfly" conformation. However, this does not account for the observation that the band is

predominantly long-axis polarized, which indicates assignment to the $1\,^1B_{2u}$ state. Moreover, Ljubić and Sabljić assigned the two features of band *B*, observed at 43300 cm^{-1} (231 nm) and 44200 cm^{-1} (226 nm) in the present study, to two different electronic states, $2\,^1B_{2u}$ and $2\,^1B_{1u}$, respectively. But assignment of the second feature to the $2\,^1B_{1u}$ state is unlikely since our polarization spectra show that both features of band *B* are long-axis polarized. The peak at 44200 cm^{-1} is most likely a vibronic component of band *B*. In general, the results of the present TD–CAM-B3LYP/AUG-cc-pVTZ calculations account well for the observed polarization spectra, but the observed long-axis polarized feature *D* with maximum at 48300 cm^{-1} (207 nm) is not easily assigned to a computed electronic state. This feature may possibly be of vibronic origin.

Acknowledgements

This investigation was supported by grants of beam time on the CD1 beamline at ISA. The stay of Nguyen Duc Duy at Roskilde University was enabled by a Ph.D. scholarship granted by the Vietnamese Ministry of Education and Training. Additional support was provided by the Danish International Development Agency (DANIDA) via the Enhancement of Research Capacity (ENRECA) program. The authors are indebted to Eva M. Karlsen for technical assistance.

The authors declare no competing financial interest.

Appendix A. Supplementary data

Supplementary data to this article can be found online at …..

Table 1

Observed features of the SRLD absorption spectrum of dibenzo-*p*-dioxin (DD) and theoretical electronic transitions predicted with TD–CAM-B3LYP/AUG-cc-pVTZ.

Observed				TD–CAM-B3LYP [a]			
	$\tilde{\nu}$ [b]	Abs [c]	Pol [d]	Term	$\tilde{\nu}$ [b,e]	f [f]	Leading configurations [g]
				$1\,^1B_{3g}$	32.2	0	95% [$3b_{3u}(\pi)\rightarrow 2a_u(\pi^*)$]
				$2\,^1A_g$	34.0	0	82% [$3b_{3u}(\pi)\rightarrow 4b_{3u}(\pi^*)$]
A	34.2	0.10	*y*	$1\,^1B_{2u}$	34.4	0.11	76% [$3b_{3u}(\pi)\rightarrow 3b_{1g}(\pi^*)$], 14% [$2b_{2g}(\pi)\rightarrow 2a_u(\pi^*)$]
				$2\,^1B_{3u}$	42.2	0.02	37% [$3b_{3u}(\pi)\rightarrow 13a_g(\sigma^*)$], 30% [$3b_{3u}(\pi)\rightarrow 15a_g(\sigma^*)$]
B	43.3	1.09	*y*	$2\,^1B_{2u}$	43.9	0.93	66% [$2b_{2g}(\pi)\rightarrow 2a_u(\pi*)$], 21% [$3b_{3u}(\pi)\rightarrow 3b_{1g}(\pi*)$]
C	47.6	0.24	*z*	$2\,^1B_{1u}$	48.1	0.31	62% [$3b_{3u}(\pi)\rightarrow 3b_{2g}(\pi*)$], 30% [$2b_{2g}(\pi)\rightarrow 4b_{3u}(\pi*)$]
D	48.3	0.21	*y*				
				$4\,^1B_{3u}$	51.3	0.03	79% [$2b_{2g}(\pi)\rightarrow 11b_{1u}(\sigma^*)$]
E	51.0	0.28	*y*	$3\,^1B_{2u}$	51.2	0.37	49% [$3b_{3u}(\pi)\rightarrow 4b_{1g}(\pi*)$], 35% [$2b_{1g}(\pi)\rightarrow 4b_{3u}(\pi*)$]
				$4\,^1B_{2u}$	52.1	0.15	46% [$2b_{1g}(\pi)\rightarrow 4b_{3u}(\pi*)$], 42% [$3b_{3u}(\pi)\rightarrow 4b_{1g}(\pi*)$]
F	52.9	0.29	*z*	$3\,^1B_{1u}$	51.8	0.18	68% [$2b_{1g}(\pi)\rightarrow 2a_u(\pi*)$], 11% [$2b_{2g}(\pi)\rightarrow 4b_{3u}(\pi*)$]
G	55.9	0.56	*z*	$5\,^1B_{1u}$	55.8	0.25	62% [$1a_u(\pi)\rightarrow 3b_{1g}(\pi*)$], 23% [$2b_{2g}(\pi)\rightarrow 5b_{3u}(\pi*)$]
				$6\,^1B_{1u}$	57.6	0.14	62% [$2b_{2g}(\pi)\rightarrow 5b_{3u}(\pi*)$], 21% [$1a_u(\pi)\rightarrow 3b_{1g}(\pi*)$]

[a] Main transitions only. Complete list of calculated transitions provided as Supplementary data S2.

[b] Peak wavenumber in 1000 cm^{-1}.

[c] Peak absorbance estimated from the partial absorbance curves in Fig. 2.

[d] Polarization direction; *y* and *z* refer to the in-plane long and short molecular axes.

[e] An empirical correction of 4000 cm^{-1} has been subtracted from the calculated wavenumber.

[f] Oscillator strength.

[g] Diagrams of π and π∗ orbitals in Fig. 3.

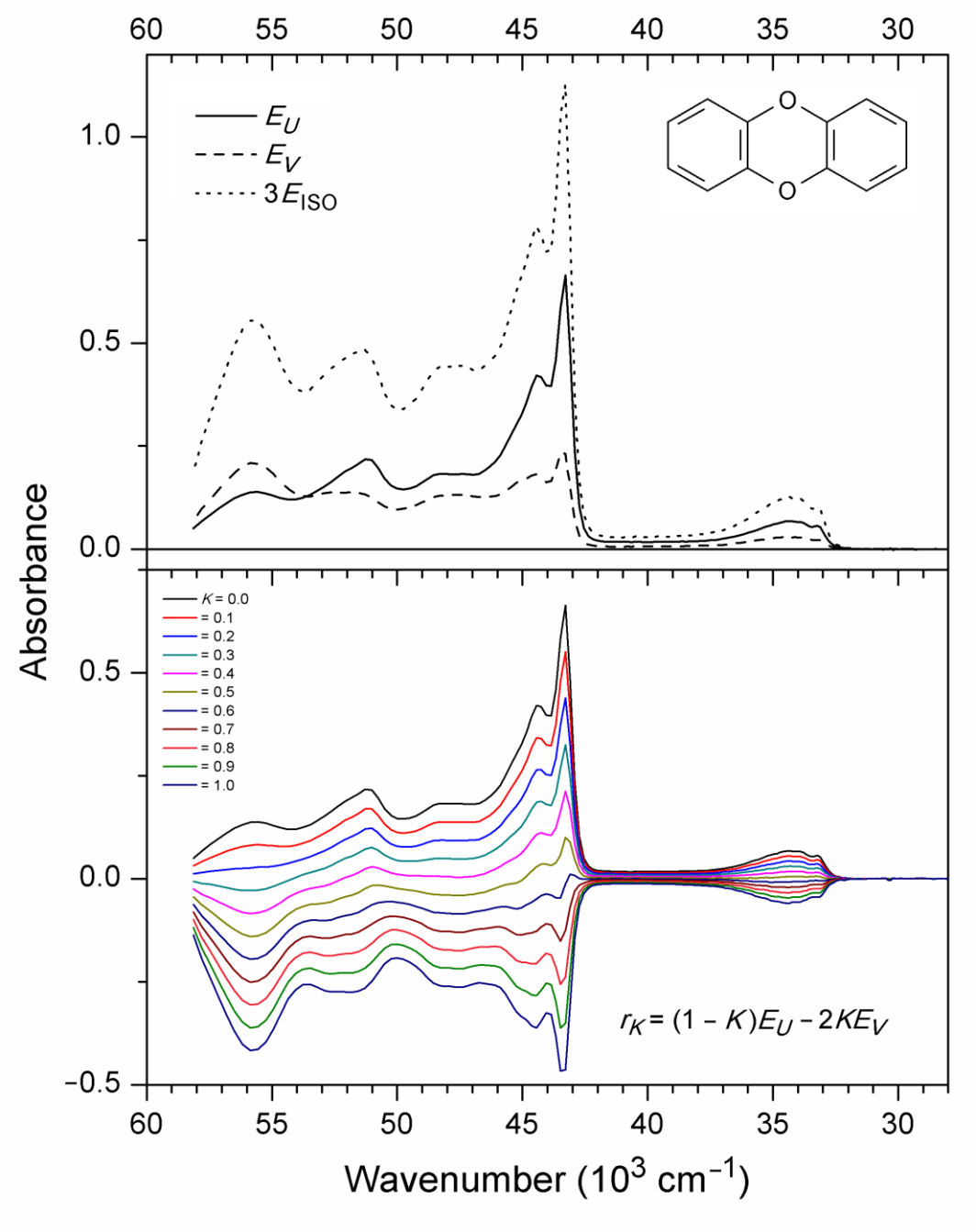

Fig. 1. *Top:* Synchrotron Radiation Linear Dichroism (SRLD) absorbance curves $E_U(\tilde{\nu})$ and $E_V(\tilde{\nu})$ for dibenzo-*p*-dioxin (DD) in stretched polyethylene measured with the electric vector of the sample beam parallel and perpendicular, respectively, to the uniaxial stretching direction U. $3E_{\mathrm{ISO}}(\tilde{\nu}) = E_U(\tilde{\nu}) + 2E_V(\tilde{\nu})$ is three times the absorbance that would have been measured in an isotropic experiment on the same sample. *Bottom:* Family of reduced absorbance curves $r_K(\tilde{\nu}) = (1 - K)E_U(\tilde{\nu}) - 2KE_V(\tilde{\nu})$ according to the TEM procedure [23,24,46] with K varying from 0 to 1 in steps of 0.1.

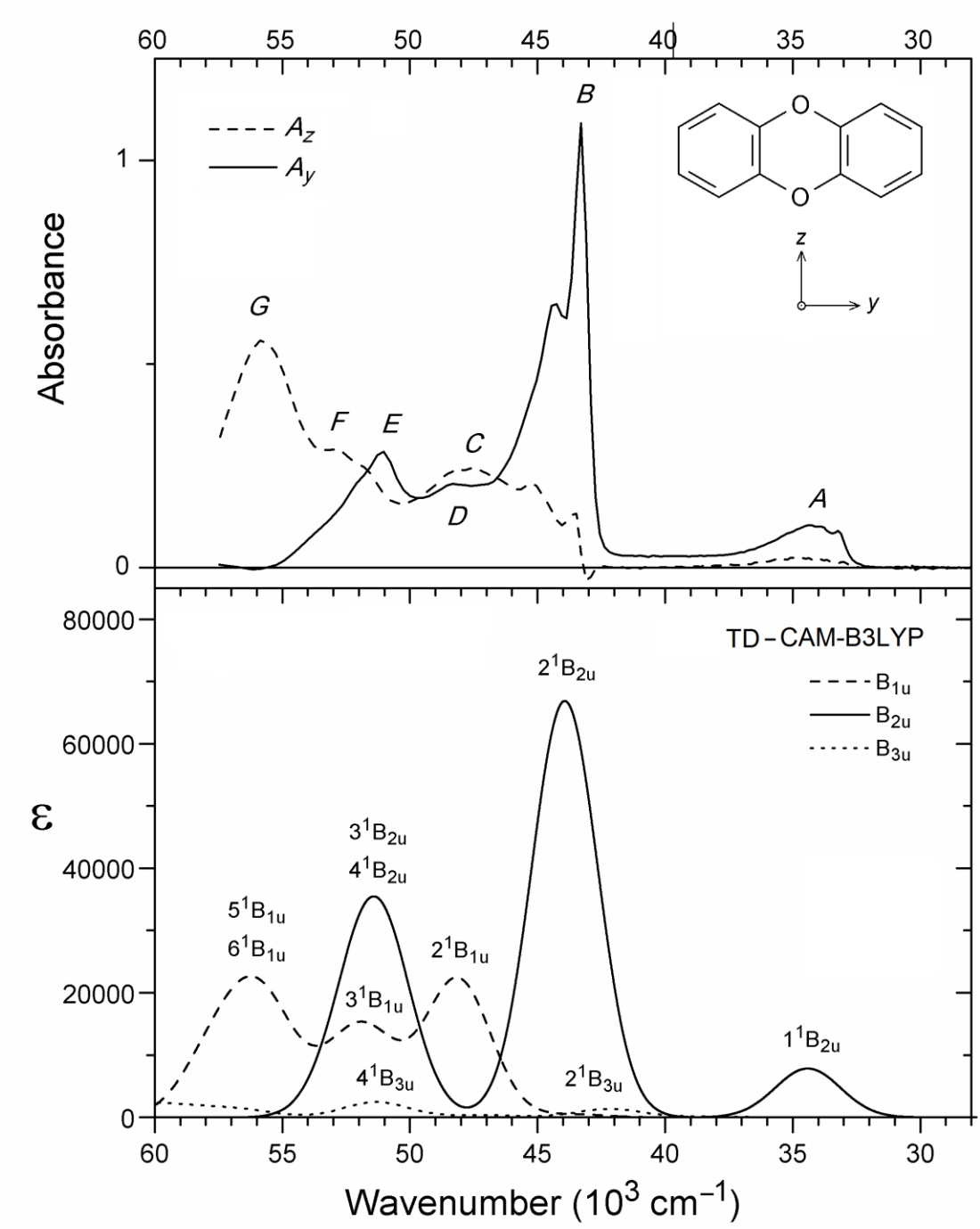

Fig. 2. *Top:* Partial absorbance curves for dibenzo-*p*-dioxin (DD). $A_z(\tilde{\nu})$ and $A_y(\tilde{\nu})$ indicate *z*- and *y*-polarized absorbance (see text). *Bottom:* Gaussian convolutions of optically allowed transitions predicted with TD–CAM-B3LYP/AUG-cc-pVTZ (see text). 4000 cm^{-1} have been subtracted from the calculated wavenumbers.

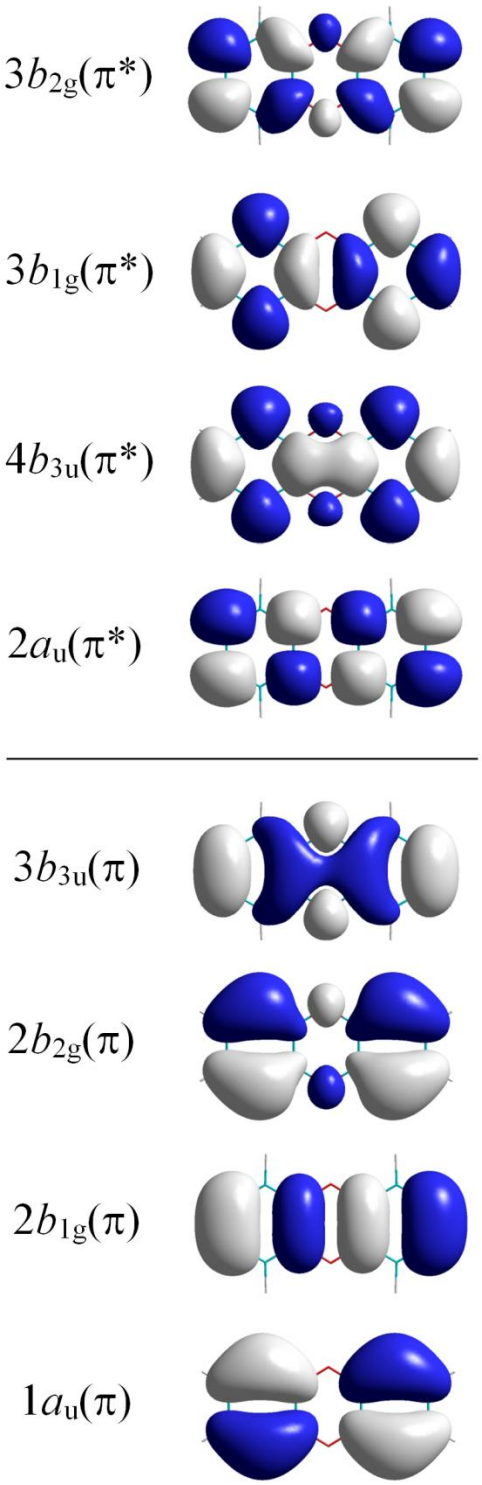

Fig. 3. Diagrams of the four highest occupied and four lowest unoccupied π type MOs for dibenzo-*p*-dioxin (DD).

References

1 S. Safe, O. Hutzinger, T.A. Hill (Eds.), Polychlorinated dibenzo-*p*-dioxins and -furans (PCDDs/PCDFs): Sources and environmental Impact, epidemiology, mechanisms of action, health risks, Springer, Berlin, Germany, 1990.

2 R.E. Alcock, K.C. Jones, Dioxins in the environment: A review of trend data, Environ. Sci. Technol. 30 (1996) 3133-3143.

3 H. Douglas, Prediction, explanation, and dioxin biochemistry: Science in Public Policy. Found. Chem. 6 (2004) 49-63.

4 A. Schecter, L. Birnbaum, J.J. Ryan, J.D. Constable, Dioxins: An overview, Environ. Res. 101 (2006) 419-428.

5 H. Zhou, A. Meng, Y. Long, Q. Li, Y. Zhang, A review of dioxin-related substances during municipal solid waste incineration, Waste Manag. 36 (2015) 106-118.

6 R. Rathna, S. Varjani, E. Nakkeeran, Recent developments and prospects of dioxins and furans remediation, J. Environ. Man. 223 (2018) 797-806.

7 A.K. Rathoure, Dioxins: Source, origin and toxicity assessment, Biodiversity Int. J. 2 (2018) 310-314.

8 S. Kanan, F. Samara, Dioxins and furans: A review from chemical and environmental perspectives, Trends Environ. Anal. Chem. 17 (2018) 1-13.

9 B. Lamotte, G. Berthier, Spectres de résonance magnétique, niveaux d'énergie et structure électronique de radicaux-cations oxygénés et soufrés d'hétérocycles aromatiques, J. Chim. Phys. 63 (1966) 369-378.

10 M.B. Ryzhikov, A.N. Rodionov, A.N. Stepanov, Spectral luminescence characteristics of the dihetero derivatives of dihydroanthracene with group VI elements, Russ. J. Phys. Chem. 63 (1989) 1378-1380.

11 E.A. Gastilovich, V.G. Klimenko, N.V. Korol'kova, R.N. Nurmukhametov, Optical spectra and photophysical properties of polychlorinated dibenzo-*p*-dioxin derivatives, Russ. Chem. Rev. 69 (2000) 1037-1056.

12 E.A. Gastilovich, V.G. Klimenko, N.V. Korol'kova, G. Rauhut, Excited electronic states and effect of vibronic-spin–orbit coupling on the radiative deactivation of the lowest triplet states of dioxins, Chem. Phys. 270 (2001) 41-54.

13 E.A. Gastilovich, V.G. Klimenko, N.V. Korol'kova, R.N. Nurmukhametov, Spectroscopic data on nuclear configuration of dibenzo-*p*-dioxin in S_0, S_1, and T_1 electronic states, Chem. Phys. 282 (2002) 265-275.

14 M. Baba, A. Doi, Y. Tatamitani, S. Kasahara, H. Kato, Sub-doppler high-resolution excitation spectroscopy of dibenzo-*p*-dioxin, J. Phys. Chem. A 108 (2004) 1388-1392.

15 J.E. Lee, W. Choi, S. Odde, B.J. Mhin, K. Balasubramanian, Electron affinity and inversion distortion of dibenzo-*p*-dioxin, Chem. Phys. Lett. 410 (2005) 142-146.

16 I. Ljubić, A. Sabljić, Dibenzo-*p*-dioxin. An ab initio CASSCF/CASPT2 study of the π–π^* and *n*–π^* valence excited states, J. Phys. Chem. A 109 (2005) 8209-8217.

17 I. Ljubić, A. Sabljić, Theoretical study of structure, vibrational frequencies, and electronic spectra of polychlorinated dibenzo-*p*-dioxins, J. Phys. Chem. A 110 (2006) 4524-4534.

18 T.K. Eriksen, B.K.V. Hansen, J. Spanget-Larsen, The vibrational structure of dibenzo-*p*-dioxin. IR linear dichroism, raman spectroscopy, and quantum chemical calculations, Polish J. Chem. 82 (2008) 921-934.

19 E.A. Gastilovich, V.G. Klimenko, N.V. Korol'kova, R.N. Nurmukhametov, A nonradiative intersystem crossing $S(\pi\pi^*) \rightsquigarrow T(\pi\pi^*)$ transition in dibenzo-*p*-dioxin, Opt. Spectrosc. 105 (2008) 820-828.

20 E.A. Gastilovich, V.G. Klimenko, L.V. Volkova, R.N. Nurmukhametov, Nonradiative deactivation of the lowest excited triplet state of the dibenzo-*p*-dioxin molecule, Opt. Spectrosc. 111 (2011) 766-775.

21 E.A. Gastilovich, V.G. Klimenko, L.V. Volkova, R.N. Nurmukhametov, The role played by some factors of intramolecular interaction in nonradiative deactivation of the lowest triplet state of octachlorodibenzo-*p*-dioxin, Opt. Spectrosc. 113 (2012) 463-473.

22 E.A. Gastilovich, V.G. Klimenko, L.V. Volkova, R.N. Nurmukhametov, Nonradiative deactivation of the lowest triplet state of tetrachlorodibenzo-*p*-dioxin, Opt. Spectrosc. 116 (2014) 368-376.

23 J. Michl, E.W. Thulstrup, Spectroscopy with polarized light. Solute alignment by photoselection, in liquid crystals, polymers and membranes, VCH-Wiley, Deerfield Beach, FL., 1986, 1995.

24 E.W. Thulstrup, J. Michl, Elementary polarization spectroscopy, Wiley-VCH, New York, Weinheim, 1989.

25 A. Rodger, B. Nordén, Circular dichroism and linear dichroism, Oxford University Press, UK, 1997.

26 B. Nordén, A. Rodger, T. Dafforn, Linear dichroism and circular dichroism: A textbook on polarized-light spectroscopy, RCS Publishing, Cambridge, UK, 2010.

27 A.J. Miles, S.V. Hoffmann, Y. Tao, R.W. Janes, B.A. Wallace, B. Synchrotron radiation circular dichroism (SRCD) spectroscopy: New beamlines and new applications in biology, Spectroscopy 21 (2007) 245-255.

28 A.J. Miles, R.W. Janes, A. Brown, D.T. Clarke, J.C. Sutherland, Y. Tao, B.A. Wallace, S.V. Hoffmann, Light flux density threshold at which protein denaturation is induced by synchrotron radiation circular dichroism beamlines, J. Synchrotron Rad. 15 (2008) 420-422.

29 D.D. Nguyen, N.C. Jones, S.V. Hoffmann, J. Spanget-Larsen, Synchrotron radiation linear dichroism (SRLD) investigation of the electronic transitions of quinizarin, chrysazin, and anthrarufin, Spectrochim. Acta A 77 (2010) 279-286.

30 P.W. Thulstrup, S.V. Hoffmann, B.K.V. Hansen, J. Spanget-Larsen, Unique interplay between electronic states and dihedral angle for the molecular rotor diphenyldiacetylene, Phys. Chem. Chem. Phys. 13 (2011) 16168-16175.

31 D.D. Nguyen, N.C. Jones, S.V. Hoffmann, S.H. Andersen, P.W. Thulstrup, J. Spanget-Larsen, Electronic states of 1,4-bis(phenylethynyl)benzene. A synchrotron radiation linear dichroism investigation, Chem. Phys. 392 (2012) 130-135.

32 P.W. Thulstrup, N.C. Jones, S.V. Hoffmann, J. Spanget-Larsen, Electronic states of the fluorophore 9,10-bis(phenylethynyl)anthracene (BPEA). A synchrotron radiation linear dichroism investigation, Chem. Phys. Lett. 559 (2013) 35-40.

33 D.D. Nguyen, N.C. Jones, S.V. Hoffmann, J. Spanget-Larsen, Vacuum UV polarization spectroscopy of *p*-Terphenyl, J. Phys. Chem. A 122 (2018) 184−191.

34 M.E. Casida, Review: Time-dependent density-functional theory for molecules and molecular solids, J. Mol. Struct. THEOCHEM 914 (2009) 3-18.

35 M.A.L. Marques, N.T. Maitra, F.M.S. Nogueira, E.K.U. Gross, A. Rubio (Eds.), Fundamentals of time-dependent density functional theory, Lecture Notes in Physics, vol. 837, Springer, Berlin, Germany, 2012.

36 H.S. Yu, S.L. Li, D.G. Truhlar, Perspective: Kohn-Sham density functional theory descending a staircase, J. Chem. Phys. 145 (2016) 130901(1-23).

37 M.J. Frisch, G.W. Trucks, H.B. Schlegel, G.E. Scuseria, M.A. Robb, J.R. Cheeseman, G. Scalmani, V. Barone, G.A. Petersson, H. Nakatsuji, X. Li, M. Caricato, A.V. Marenich, J. Bloino, B.G. Janesko, R. Gomperts, B. Mennucci, H.P. Hratchian, J.V. Ortiz, A.F. Izmaylov, J.L. Sonnenberg, D. Williams-Young, F. Ding, F. Lipparini, F. Egidi, J. Goings, B. Peng, A. Petrone, T. Henderson, D. Ranasinghe, V.G. Zakrzewski, J. Gao, N. Rega, G. Zheng, W. Liang, M. Hada, M. Ehara, K. Toyota, R. Fukuda, J. Hasegawa, M. Ishida, T. Nakajima, Y. Honda, O. Kitao, H. Nakai, T. Vreven, K. Throssell, J.A. Montgomery, Jr., J.E. Peralta, F. Ogliaro, M.J. Bearpark, J. J. Heyd, E.N. Brothers, K.N. Kudin, V.N. Staroverov, T.A. Keith, R. Kobayashi, J. Normand, K. Raghavachari, A.P. Rendell, J.C. Burant, S.S. Iyengar, J. Tomasi, M. Cossi, J.M. Millam, M. Klene, C. Adamo, R. Cammi, J. W. Ochterski, R.L. Martin, K. Morokuma, O. Farkas, J.B. Foresman, D.J. Fox, GAUSSIAN16, Revision A.03, Gaussian, Inc., Wallingford CT, 2016.

38 A.D. Becke, Density-functional thermochemistry. II. The effect of the Perdew-Wang generalized-gradient correlation correction, J. Chem. Phys. 97 (1992) 9173-9177.

39 A.D. Becke, Density-functional thermochemistry. III. The role of exact exchange, J. Chem. Phys. 98 (1993) 5648-5652.

40 C. Lee, W. Yang, R.G. Parr, Development of the Colle-Salvetti correlation-energy formula into a functional of the electron density, Phys. Rev. B 37 (1988) 785-789.

41 T.H. Dunning, Jr., Gaussian basis sets for use in correlated molecular calculations. I. The atoms boron through neon and hydrogen, J. Chem. Phys. 90 (1989) 1007-1023.

42 R.A. Kendall, T.H. Dunning, Jr., R.J. Harrison, Electron affinities of the first-row atoms revisited. Systematic basis sets and wave functions, J. Chem. Phys. 96 (1992) 6796-6806.

43 T. Yanai, D. Tew, N.A. Handy, New hybrid exchange-correlation functional using the Coulomb-attenuating method (CAM-B3LYP), Chem. Phys. Lett. 393 (2004) 51-57.

44 S. Grimme, Calculation of the electronic spectra of large molecules, Rev. Comput. Chem. 20 (2004) 153-218.

45 A. Serr, N. O'Boyle, Convoluting UV-Vis spectra using oscillator strengths (July 13, 2009). Available from http://gausssum.sourceforge.net/GaussSum_UVVis_Convolution.pdf.

46 F. Madsen, I. Terpager, K. Olskær, J. Spanget-Larsen, Ultraviolet-visible and infrared linear dichroism spectroscopy of 1,8-dihydroxy-9,10-anthraquinone aligned in stretched polyethylene, Chem. Phys. 165 (1992) 351-360.